ULTRASONIC ACOUSTIC FIELD HOMOGENEITY IN THE NEAR FIELD OF TRANSDUCERS

Liliana GHEGOIU[1], Cristian-Cătălin PETRE[2], Mihai Valentin PREDOI [3*]

Ultrasonic longitudinal-wave transducers (LWTs) are widely employed across a broad range of scientific and technological applications. Despite their critical role in the characterization of nanoparticle suspensions, the acoustic behavior within their near-field region remains insufficiently explored in existing literature. In this study, a systematic analysis is conducted to identify the conditions and parameters governing the homogeneity of the acoustic field in the near field of ultrasonic transducers. Both the theoretical principles underlying wave propagation in this region and the practical implications for transducer design and optimization are examined. The investigation is supported by experimental and numerical simulations, including finite element analysis (FEA), to provide a comprehensive understanding of near-field acoustic phenomena.

Keywords: ultrasonic transducer, near field, acoustics numerical simulation.

1. Introduction

Classical investigations of acoustic field formation have demonstrated that spatial inhomogeneities in the velocity distribution across the transducer surface give rise to significant pressure perturbations within the near-field region. The study by Hutchins et al. [1] provides both experimental and numerical evidence that deviations from acoustic field uniformity arise even in idealized circular transducers, primarily due to diffraction effects and localized variations in vibrational behavior. Furthermore, the authors show that the near-field pressure distribution is characterized by a complex pattern of alternating high- and low-intensity regions. This nonuniform structure has a direct impact on the transducer's capacity to generate a well-defined and stable acoustic beam in the far field. The significance of near field nonuniformity has been emphasized

* Corresponding author
[1] Ph.D. candidate, Dept. of Mechanics, National University of Science and Technology POLITEHNICA Bucharest, Romania,ghegoiuliliana@gmail.com
[2] Prof., Dept. of Strength of Mat., National University of Science and Technology POLITEHNICA Bucharest, Romania, cristianpetre60@gmail.com
[3*] Prof., Dept. of Mechanics, National University of Science and Technology POLITEHNICA Bucharest, Romania, mihai.predoi@upb.ro

in foundational studies on acoustic radiation from piston sources. Stepanishen [2] analyzed the impulse response of a piston transducer and demonstrated that the near-field pressure distribution is governed by the complex interplay among surface motion, propagation time, and piston geometry. His results indicate that, in this region, the acoustic pressure exhibits pronounced temporal and spatial variations, and the wavefront undergoes substantial distortion prior to the establishment of a stable far-field beam. Consequently, the uniformity of the near field emerges as a critical determinant of the shape and stability of the resulting ultrasonic beam. Subsequently, Greenspan [3] extended the theory of rigid piston radiation by considering nonuniform vibrational velocity distributions, including parabolic, clamped, simply supported, and Gaussian profiles. His findings reveal that Gaussian velocity distributions yield significantly more uniform near-field patterns compared to those associated with rigid piston assumptions or other boundary conditions. In particular, the characteristic oscillatory structure of the near field is markedly attenuated under Gaussian excitation, suggesting a viable design strategy for enhancing field homogeneity. These results underscore that acoustic radiation from a piston is not solely determined by its geometry but is strongly influenced by the spatial distribution of the imposed surface velocity. The adoption of idealized Gaussian profiles thus provides both a theoretical and practical framework for the design of modern transducers with controlled nonuniform excitation. Contemporary applied studies further corroborate the importance of near-field effects. High-frequency (50 MHz) medical transducers, such as those investigated by Khameneh et al. [4], exhibit a strong dependence on near-field homogeneity, as imaging resolution is directly linked to pressure uniformity prior to acoustic focusing. Similarly, flexible composite transducers examined by Hou et al. [5] introduce additional sources of near-field variability arising from localized deformability of the piezoelectric surface. In industrial contexts, studies such as those by Metzenmacher et al. [6] demonstrate that near-field inhomogeneities generated at the transducer surface can propagate and be further amplified through reflections from rigid boundaries, thereby degrading system sensitivity—for example, in fluid level measurements within curved metallic vessels.

Taken together, these contributions highlight that the homogeneity of the ultrasonic acoustic field in the near field constitutes a fundamental prerequisite for the formation of a stable, coherent, and predictable beam. In the absence of a detailed understanding of this region, the optimization of transducer performance remains inherently limited, with direct implications for medical, industrial, and research applications.

In this context, the present study provides a systematic analysis of the conditions and parameters governing the homogeneity of the acoustic field in the near field generated by ultrasonic transducers mounted within a container for the characterization of nanoparticle suspensions. Both the theoretical foundations of wave propagation in this region and the practical implications for transducer design and optimization are addressed.

2. Theoretical model

Ultrasonic transducers immersed in liquids—particularly in water—generate an acoustic near field that must be spatially uniform for applications such as particle characterization. The acoustic field in front of a circular piston-like transducer can be obtained as an integral on the surface of the transducer, each elementary surface acting as an acoustic monopole source (Fig. 1). More details can be found in refs. [7] (Sect. 7.4), or [8].

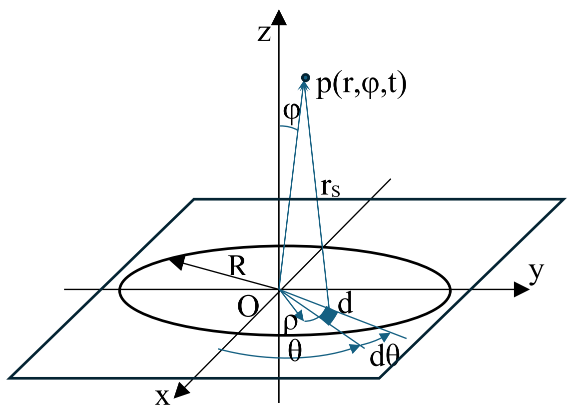

Fig. 1 Geometric domain of acoustic radiation

The surface *S* of the transducer is considered to act as baffled circular piston (inserted in a rigid fixed wall) and moves uniformly with a harmonic velocity $U_0 \exp(i\omega t)$ along the Oz direction. The velocity amplitude is denoted U_0 on the surface of the piston, $\omega = 2\pi f$ is the angular frequency (*f* = frequency in Hz), and $i = \sqrt{-1}$. Each elementary surface *dS* of the piston acts as a baffled simple source of intensity $dQ = U_0 dS$ (Fig. 1). The acoustic pressure $p(r,\varphi,t)$ at a point in the fluid - specified by its radial distance *r* from the center of the piston and its azimuthal angle φ - within a medium characterized by mass density ρ_0 and sound speed c_0, is [7]:

$$p(r,\varphi,t) = i\rho_0 f U_0 e^{-i\omega t} \int_S \frac{\exp(ikr_s)}{r_s} dS \,. \qquad (1)$$

The wave number is $k=\dfrac{\omega}{c_0}$ and the propagating factor of the wave is expressed as: $\exp\left[i\left(kr-\omega t\right)\right]$ and $r_s^2=r^2-2\rho r\sin\varphi+\rho^2$.

2.1. Acoustic pressure along the symmetry axis

The acoustic pressure along the symmetry axis Oz (φ=0), remarking that $r_s=\sqrt{r^2+\rho^2}$, can be determined analytically as an integral of radial coordinate ρ only:

$$p\left(r,0,t\right)=2\pi i\rho_0 fU_0 e^{-i\omega t}\int_0^R \frac{\exp\left(ik\sqrt{r^2+\rho^2}\right)}{\sqrt{r^2+\rho^2}}\rho d\rho . \qquad (2)$$

It can be proven that $\dfrac{d}{d\rho}\left\{\exp\left(ik\sqrt{r^2+\rho^2}\right)\right\}=ik\dfrac{\rho\exp\left(ik\sqrt{r^2+\rho^2}\right)}{\sqrt{r^2+\rho^2}}$, so that the acoustic pressure given by eq. (2) on the symmetry axis, becomes:

$$\begin{aligned} p\left(r,0,t\right)&=\frac{\omega}{k}\rho_0 U_0 e^{-i\omega t}\left[\exp\left[ik\sqrt{r^2+\rho^2}\right]\right]_0^R \\ &=c_0\rho_0 U_0\left\{\exp\left[ikr\left(\sqrt{1+\left(\frac{R}{r}\right)^2}-1\right)\right]-1\right\}e^{i\left(kr-\omega t\right)} \end{aligned} \qquad (3)$$

This acoustic pressure of a plane wave, as given by eq. (3) is a complex function, providing information about the acoustic pressure amplitude P and its local phase. The absolute value P of the complex expression (3) depends on the axial position r:

$$P\left(r,0\right)=2c_0\rho_0 U_0\left|\sin\left\{\frac{kr}{2}\left(\sqrt{1+\left(\frac{R}{r}\right)^2}-1\right)\right\}\right| \qquad (4)$$

It follows that the acoustic pressure amplitude depends on the axial position and has local minima for $\frac{kr}{2}\left(\sqrt{1+\left(\frac{R}{r}\right)^2}-1\right)=n\pi;\; n=0,1,2,...$ These minima are produced by interference of partial waves and could be affecting the sensitivity of diphasic fluids inspection, especially in the vicinity of these minima. On the other hand, the first maximum is obtained for $\sqrt{1+\left(\frac{R}{r}\right)^2}-1=\frac{\pi}{kr}$. For large distances r>>R the approximation $\sqrt{1+\left(\frac{R}{r}\right)^2}\approx 1+\frac{1}{2}\left(\frac{R}{r}\right)^2$ holds and the distance $r=H$ at which this first maximum occurs is called the Fresnel distance by some authors or Rayleigh length by others [7]. The distance $r=N$ between the transducer's surface and this particular point of maximum pressure, represents the acoustic near field in which all maxima and minima of acoustic pressure are located. With good approximation for r>>R : $\sqrt{1+\left(\frac{R}{r}\right)^2}-1\approx\frac{1}{2}\left(\frac{R}{r}\right)^2=\frac{\pi}{kr}$ leading to $r=N=\frac{kR^2}{2\pi}=\frac{R^2}{\lambda}$ in which $\lambda=\frac{2\pi}{k}=\frac{c_0}{f}$ is the wavelength. In the near field exist all pressure minima/maxima indicated above.

The practical incident acoustic signal is a multifrequency amplitude modulated signal. Therefore, the acoustic signal will be transformed into its frequency spectrum and for each pair $\{f_i, U_{0i} : i=1\ldots n\}$ the acoustic pressure will be given by eq. (4). The effective acoustic pressure is the sum of these n partial acoustic pressures, with n sufficiently large to include all signals with amplitudes larger than $\frac{1}{2}\max_i\left(U_{0i}\right)$ or covering a sufficiently large frequency bandwidth. This analysis is presented in the Numerical results section.

2.2. Acoustic pressure lobes

Not only the axial acoustic pressure distribution is critical, but the beam divergence angle and the presence of side lobes are equally important parameters. Excessive beam divergence may compromise the objective of achieving a uniform acoustic pressure field between the immersed transducers. The acoustic pressure in a point of position given by its radial distance r and azimuthal angle φ was deduced in ref. [7], emphasizing the role of the product kR:

$$p(r,\varphi,t)=\frac{i}{2}\rho_0 c_0 U_0 \frac{R}{r}(kR)\left[\frac{2J_1(kR\sin\varphi)}{kR\sin\varphi}\right]\exp^{i(kr-\omega t)} \quad . \tag{5}$$

The quantity in brackets represents the angular dependence of the acoustic pressure radiated by the circular transducer. Cancelling this quantity implies the conical frontier between lobes. There is always a central lobe, and its φ_1 cone angle represents the divergence of the beam. This angle and the successive separation angles of the secondary lobes will be determined in the numerical example section and shown on Fig. 6 for a series of frequencies and a given radius R of the transducer. More information is obtained by Finite Elements Analysis (FEA) in the fourth section.

3. Experimental frequency spectrum

The acoustic pressure amplitude and the angular extent of the acoustic lobes both depend on the frequency of the transducer's produced excitation. The transducers used in experiments have a central frequency and a certain bandwidth which is defined as the frequency range for which the spectral amplitudes are above half the maximum amplitude determined at the central frequency.

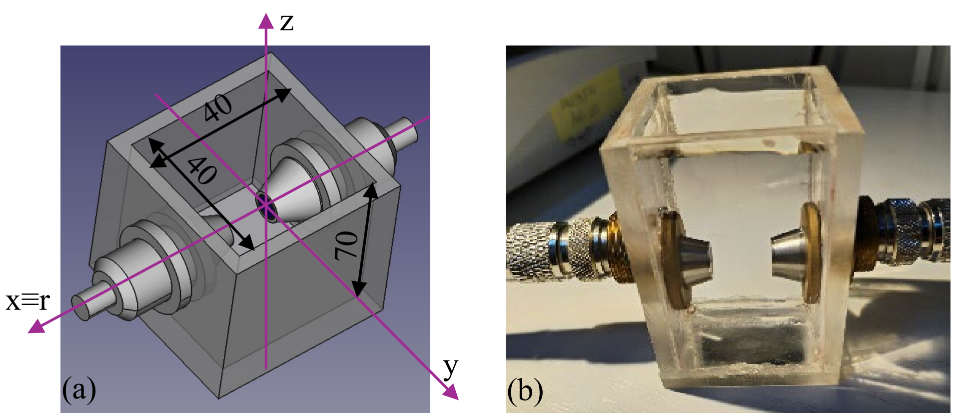

Fig. 2 The ultrasonic transducers analyzed in the present article. Perspective view of the model (a) and image of the experimental setup (b)

The recorded ultrasonic pulse generated and received by two coaxial identical longitudinal wave transducers (LWT) is shown on Fig. 2. Both are of type Olympus Panametrix V324-SU with a piezoelectric element of 6 mm diameter, inserted in a 12 mm casing.

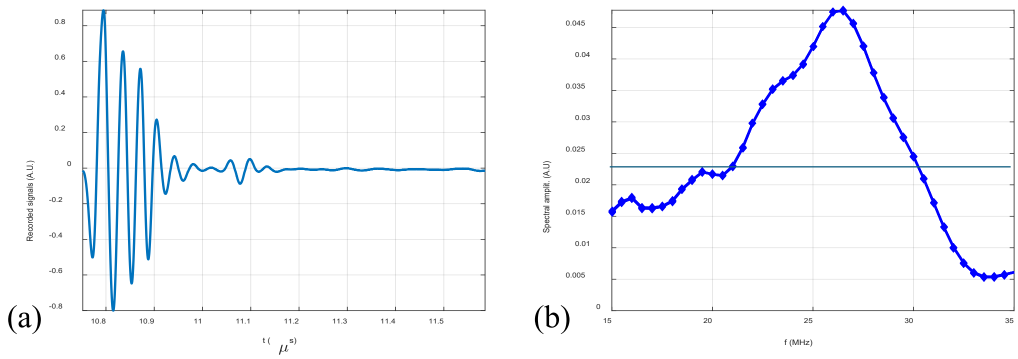

Fig. 3 Experimental determined acoustic pulse (a) and its frequency spectrum (b)

The acoustic signal shown on (Fig. 3a) has the frequency spectrum (Fig. 3b) as obtained by Fast Fourier Transform (FFT) code, implemented in MATLAB [9].

The selected spectral amplitudes are marked as dots on Fig. 3b and are used as input data for the numerical simulation of the piston model of the transducer in the free field. The spectral components are chosen to cover the typical bandwidth of the transducer down to half of the signal's maximum amplitude, marked by a horizontal line on Fig. 3b.

4. Numerical results for the acoustic field

4.1. Application of the theoretical model

The acoustic pressure amplitude P along the axis of the transducer, given by analytical eq. (4) depends only on the axial coordinate *r*, meaning that the acoustic wave propagating from the circular transducer exhibits clearly located minima for any moment of time.

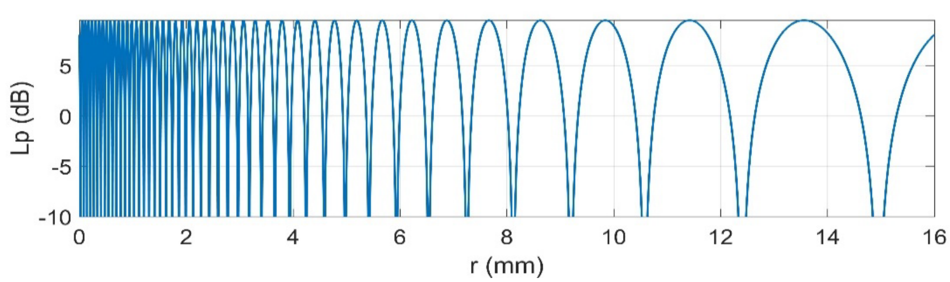

Fig. 4 Acoustic pressure level along axis for a transducer of f =25 MHz and radius R=3 mm

Based on input data from the experimental part, a transducer with central frequency of 25 MHz and radius R = 3 mm exhibits acoustic pressure as shown on Fig. 4. The resulting acoustic pressure level proves the uniformity of the peaks, but close to the limit value of 16 mm, the zones with lower acoustic pressure extend to the order of millimeters. This means that a permanent signal of pure frequency 25 MHz produces in the near field, numerous zones with reduced pressure, inadequate for practical experiments. The next step in the numerical simulation is to use the experimental frequency spectrum shown in Fig. 3b. Using formula (4) for each pair frequency – amplitude $\{f_i, U_{0i} : i=1\ldots21\}$ scaled to obtain similar order of magnitude for the mean acoustic pressure, the cumulated total acoustic pressure amplitude $P(r)=\sum_{n=1}^{21} P_n(r)$ along the axis of the transducer is plotted on Fig. 5.

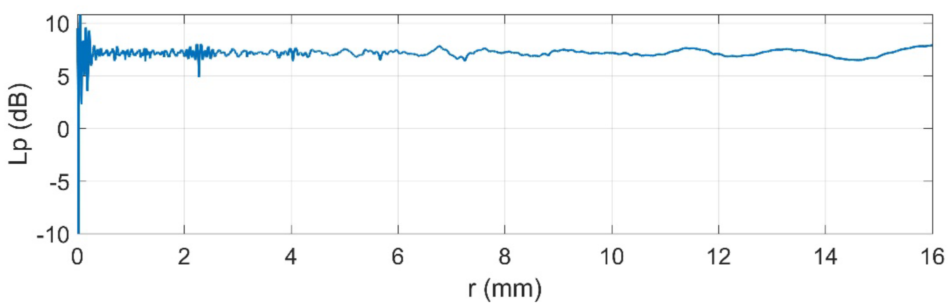

Fig. 5 Acoustic pressure level along 16mm for a real transducer based on the measured frequency spectrum.

The acoustic pressure along the transducer's axis is determined using the formula (4) and converted in dB according to: $L_{dB} = 20\log\frac{p}{p_{ref}}$ with p_{ref} = 1 μPa (Fig. 4). The central frequency of a transducer is f=25 MHz, radius R = 3 mm and it is considered a surface velocity of amplitude U_0 =1 pm/s. The sound velocity in pure water (ρ=1000 kg/m3) at 23°C is c_0=1490 m/s.

One important remark is that for this transducer, for a stationary acoustic wave with given spectral profile, the resulting acoustic pressure in the near field is relatively constant (deviations les than +/- 0.5dB about the average), with two exceptions:

a) very close (0.3 mm) to the transducer, there is a localized minimum of acoustic pressure.

b) between 2.1 and 2.5 mm distance of the transducer there is a fluctuation of 3 dB.

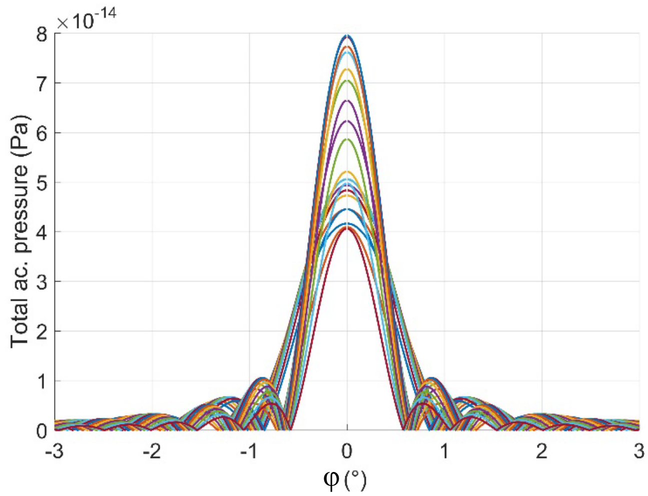

Fig. 6 Angular dependence of the acoustic pressure radiated for each spectral amplitude obtained from the experiment.

According to eq. (5), the angular dependence of the acoustic pressure radiated by the circular transducer is presented in Fig. 6 for each of the 21 selected components of the signal. The central lobe has a divergence of less than 0.4° at half-amplitude of each plot. Consequently, the beam may be regarded as well-collimated, exhibiting an approximately cylindrical profile, which constitutes a favorable characteristic for experimental applications.

4.2. FEA of the acoustic field in front of the transducer

The finite element analysis (FEA) was performed using COMSOL Multiphysics 5.1 [10], employing a custom-implemented acoustics model based on the axial symmetry of the geometry. The acoustic domain consists of water, while the circular transducer is modeled as a radial segment of radius R located on the base having the origin on the symmetry axis, thus generating the surface corresponding to a piston-type source.

Simulations were conducted in the frequency domain, with a spatial discretization ensuring a minimum of five finite elements per wavelength to achieve adequate resolution of the acoustic field. To approximate free-field conditions, non-reflecting (absorbing) boundary conditions were applied at sufficiently large distances from the source, ensuring that the computational domain fully encompasses the region of interest without introducing spurious reflections.

4.3. The near acoustic field of LWT determined by FEA

The FEA model is axially symmetric, represented by a rectangular domain of radius *Re* =6mm and height H=16mm. The LWT is represented by a segment of R=3 mm, which by rotation around the symmetry axis represents the circular surface of the transducer. The fluid domain is divided into 960000 square elements of 0.01 mm edge.

The main issue a FEA user encounters is how to apply the boundary conditions, since the active surface of the transducer surface can be modeled: either as a harmonic pressure $P_0 \exp(-i\omega t)$, or as an acceleration $A_0 \exp(-i\omega t)$, in which P_0 is the pressure amplitude (Pa) and A_0 is the surface acceleration (m/s^2). The surface velocity is in harmonic motion $\dot{U}_0 \exp(-i\omega t)$, thus the acceleration amplitude will be $A_0 = \omega \dot{U}_0$, value which has been used to obtain the pressure level shown on Fig. 7a.

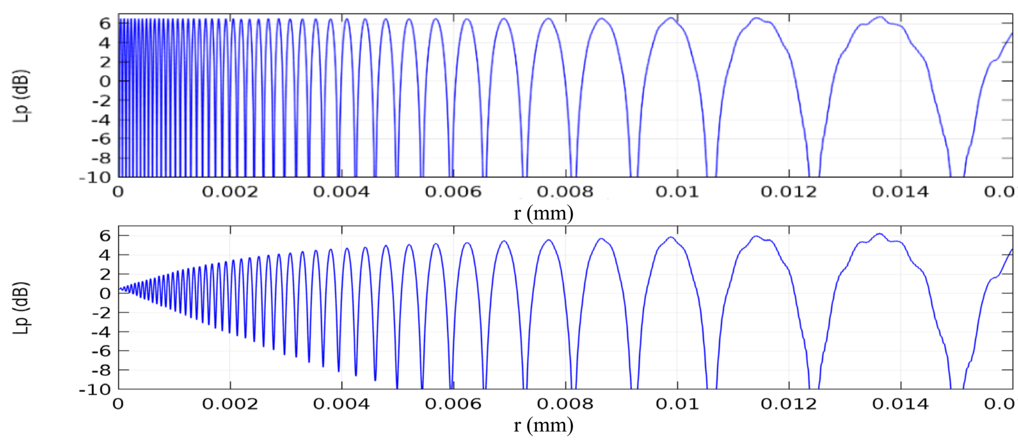

Fig. 7 The pressure level along the symmetry axis f=25 MHz, excitation by acceleration A_0 (a) and by pressure P_0 (b) obtained by FEA.

The results compare well with the analytical results shown on Fig. 4, with very small amplitude jitter beyond 10 mm from the surface of the transducer. These artefacts are due to the elements size which should be smaller for a better accuracy. On the other hand, for plane waves since $\rho_0 \ddot{U}_0 = -\frac{\partial p}{\partial x} \Rightarrow i\rho_0 \omega \dot{U}_0 = -ikP_0 \Rightarrow P_0 = \rho_0 c_0 \dot{U}_0$ which is the corresponding harmonic pressure which can be applied to the surface of the transducer.

Applying the pressure as boundary condition, the obtained result (Fig. 7 b) is different from the previous result, especially near the transducer's surface (<6 mm), which is considered as an imperfect numerical solution.

A more general view of the acoustic field in axial cross-section is shown on Fig. 8. It is a visible difference in the pressure acoustic field produced by the two approaches. The boundary condition on the variable of the problem is a Dirichlet type of boundary condition, imposing the values of the acoustic pressure along the boundary representing the piston-like transducer. Or, in the close vicinity of the piston center, the pressure is P_0= 1.49 µPa and as the distance along the axis increases, the other elementary areas of the piston contribute to the total pressure. In fact, at distances over 6 mm, the results are almost coincidence.

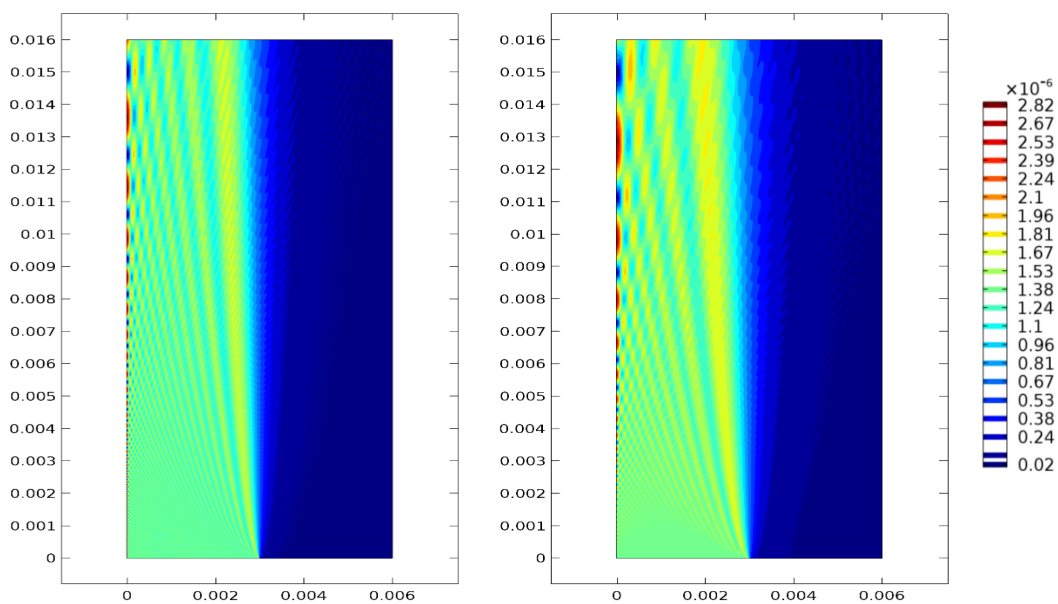

Fig. 8 Acoustic pressure amplitude in the liquid domain f=25 MHz, excitation by acceleration A_0 (a) and by pressure P_0 (b). Color bar in Pa, for both plots.

On the other hand, an acceleration boundary condition is a von Neumann type of boundary condition, pertaining to the derivative of the variable, which is a softer condition. These observations demonstrate that applying excitation boundary conditions in terms of acceleration is preferable for obtaining an accurate solution across the entire acoustic domain.

Another observation from Fig. 8 s is the presence of elongated, yellow, ray-like features of lower amplitude, suggesting the existence of an apparent acoustic source located at the junction between the transducer and the rigid wall. In practice, however, a viscoelastic rubber ring is present between the piezoelectric disc of radius R and the steel casing of radius *Re*.

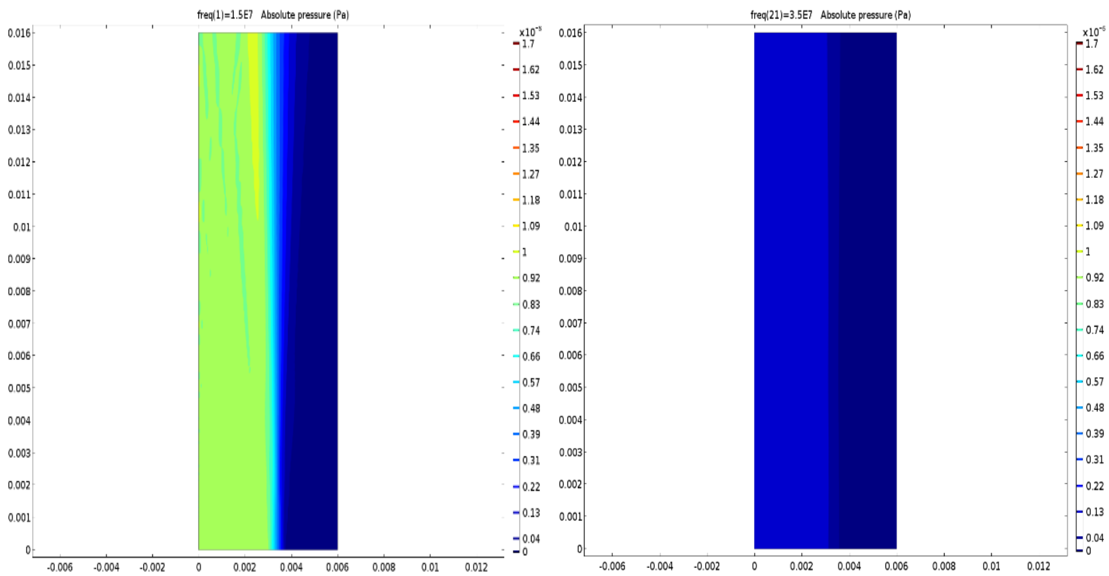

Fig. 9 Acoustic pressure amplitudes for 15 MHz (a) and 35 MHz (b) and corresponding amplitudes.

In order to asses a realistic ultrasonic acoustic field, an iterative the FEA analysis was performed in the frequency domain, for the 21 pairs frequency/amplitude around the central frequency of 25 MHz, extracted from the frequency spectrum shown on Fig. 3 b. The limit cases with their corresponding modal amplitudes are shown on Fig. 9 as plots of absolute acoustic pressures.

The FEA numerical values representing the surface plots of the 21 figures (size of 37 MB each), such as the extreme ones shown on Fig. 9, were extracted in the FEM domain (D) and summed: $P(r,\varphi)=\sum_{n=1}^{21} P_n(r,\varphi);\,(r,\varphi)\in D$, using a numerical code developed by the authors in MATLAB [9]. The resulting ultrasonic acoustic pressure field (absolute magnitude), shown in Fig. 10, reveals a uniformly insonified region (plotted in yellow) that is clearly delineated from the surrounding low-pressure (free) zone (plotted in blue).

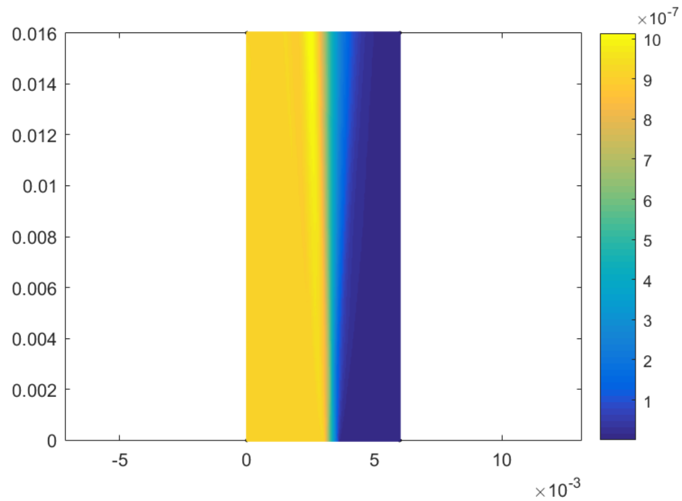

Fig. 10 Effective acoustic pressure for the given transducer

This result proves that the ultrasonic insonification in the near field for a transducer of 25 MHz central frequency is sufficiently uniform for diphasic fluid characterization, fact proven by the relative standard deviation $\frac{\sigma}{\overline{p}}(\%)$ of the acoustic pressure has in the insonified domain (r < R) which is of 3.1 %, with σ representing the standard deviation of the computed acoustic pressure, relative to the mean acoustic pressure $\overline{p}$ in this domain. This conclusion is important for ultrasonic characterization of fluids with nanoparticles in suspension.

5. Conclusions

The longitudinal waves transducers are usually modeled as axially translating pistons, with harmonic motion and inherent zones of low acoustic pressure appearing in the near field. This work investigated the realistic case of a LWT which is producing short signals. The associated discrete frequency spectrum (FFT) was determined for a signal produced by a real transducer. In this case, the superposition in the near field of individual solutions for each frequency in the spectrum, was proven to produce a relatively uniform pressure distribution on the axis of the LWT. The FEA of the acoustic field revealed that excitation of the piezoelectric element should be modeled as imposed acceleration for an overall accurate result. The inclusion in the FEA model of the existing connecting elastomeric ring, between the piezoelectric disc and the steel casing, produces significant improvements in the uniformity of the generated acoustic field, but this detail remain to be investigated in further works. A full acoustic domain superposition of obtained total acoustic pressure by FEA, for the selected set of spectral components, proves the uniformity of the insonification between the coaxial transducers, fact which is of utmost interest for experiments in small containers with biphasic fluids.

R E F E R E N C E S

[1] *D. Hutchins, H. Mair, P. Puhach and A. Osei*, "Continuous-wave pressure fields of ultrasonic transducers," J. Acoust. Soc. Am., vol. 80, no. 1, p. 12, 1986.

[2] *P. Stepanishen*, "The Time-Dependent Force and Radiation Impedance on a Piston in a Rigid Infinite Planar Baffle," J. Acoust. Soc. Am., vol. 49, no. 3B, pp. 841-849, 1971.

[3] *M. Greenspan*, "Piston radiator: Some extensions of the theory," J. Acoust. Soc. Am., vol. 65, no. 3, pp. 608-621, 1979.

[4] *A. Khameneh, H. Pishkenari and H. Chaboc*, "Optimized integrated design of a high-frequency medical ultrasound," Applied Sciences SN, vol. 3, no. 650, 2021.

[5] *C. Hou, Z. Li, C. Fei, Y. Li, Y. Yang, T. Zhao, Y. Quan, D. Chen, X. Li, W. Bao and Y. Yang,* "Active acoustic field modulation of ultrasonic transducers with flexible composites," Communications physics, vol. 6, no. 252, 2023.

[6] *M. Metzenmacher, A. Beugholt, D. Geier and T. Becker*, "Combined Longitudinal and Surface Acoustic Wave Analysis for Determining Small Filling Levels in Curved Steel Containers," MDPI, vol. 22, no. 9, 2022.

[7] *L. Kinsler, A. Frey, A. Coppens and J. Sanders,* Fundamentals of Acoustics, New York: J. Wiley & Sons, Inc., 2000.

[8] *X. Fan, E. Moros and W. Straube*, "Acoustic field prediction for a single planar continuous wave source using an equivalent phased array method," J. Acoust. Soc. Am., vol. 102, no. 5, p. 2734–2741, 1997.

[9] ***, "Matab R2025a," MathWorks, [Online]. Available: https://www.mathworks.com/products/matlab.html. [Accessed 2026].

[10] ***, "COMSOL Multiphysics," COMSOL, Inc. 100 District Avenue, Burlington, USA, 2025. [Online]. Available: https://www.comsol.com/. [Accessed 2025].